Investigating the coupling between transport and reaction within a catalyst pellet using *operando* magnetic resonance spectroscopic imaging

Scott V. Elgersma[a,1], Jordan A. Ward-Williams[a], Qingyuan Zheng[a], Andrew J. Sederman[a], Michael D. Mantle[a], Constant M. Guédon[b], Lynn F. Gladden[a*]

a. Magnetic Resonance Research Centre, Department of Chemical Engineering & Biotechnology, University of Cambridge, Philippa Fawcett Drive, Cambridge CB3 0AS, United Kingdom

b. Shell Global Solutions International B.V., Grasweg 31, Amsterdam 1031 HW, The Netherlands

*Corresponding author email: lfg1@cam.ac.uk

[1] Present Address: Shell International Petroleum Company, Shell Centre, York Road, London SE1 7NA, United Kingdom

Abstract

In heterogeneous catalysis, the distribution of reactant and product species within a catalyst pellet are of central importance to the catalyst performance, and ultimately to the overall conversion and selectivity achieved in commercial-scale reactors. Despite this importance, fundamental understanding of pellet scale behaviour at *operando* conditions is limited due to the coupled, multi-scale nature of the underlying transport processes, and the limited techniques capable of mapping the intra-pellet composition at industrially relevant length scales. Here, we demonstrate the coupling between transport and reaction at the pellet scale by using *operando* magnetic resonance spectroscopic imaging (MRSI) to map the liquid composition within Pd/γ-Al_2O_3 catalyst pellets at an isotropic in-plane spatial resolution of 86 μm during a styrene hydrogenation reaction. The results reveal that asymmetric liquid wetting at the pellet surface, typical of that occurring in trickle-bed reactors, causes significant composition heterogeneity across a catalyst pellet. Due to the wetting inhomogeneity, commonly used 1D reaction-diffusion models are inadequate for describing the observed composition heterogeneity across the pellet. The results reported here provide unique experimental insight into the coupling between transport and reaction at the pellet scale within an operating reactor.

Keywords: MRI, NMR, operando, heterogeneous catalysis, wetting, mass transfer

1 Introduction

The distribution of reactant and product species within a catalyst pellet are of central importance to the catalyst performance, and ultimately to the overall conversion and selectivity achieved in commercial-scale reactors, since the local molecular concentration experienced by catalytic active sites will dictate the local reaction kinetics. Further, the intra-pellet composition will influence the diffusion and adsorption processes occurring within the pellet. To effectively utilize the catalyst pore space, it is desired that the reactant can readily access the entire intra-pellet space, and that products, once formed, rapidly diffuse out of the pellet. The degree to which a pellet is effectively utilized depends on the pellet size, pellet shape, the diffusivity of the reactant and products, and the mass transfer conditions at the pellet surface. Clearly, these are pellet-scale properties. Thus, to understand and subsequently optimize catalyst pellets, measurements of composition at the pellet-scale are required. However, due to limitations of standard catalysis techniques and spectroscopies, most *operando* measurements of composition to date have been made at length-scales far smaller than the pellet scale (e.g. measurements using catalyst crystals or powders) [1,2].

Magnetic resonance techniques are uniquely capable of quantitatively measuring the concentration of species within catalyst pellets at industrially-relevant length scales [3–5]. Such measurements of the intra-pellet concentration have given new insights into the behaviour within industrially-relevant catalysts in operating packed- and trickle-bed reactors [6–11]. However, to date, most magnetic resonance measurements of intra-pellet composition have been made at a spatial resolution too low to permit the investigation of the concentration profile within individual pellets. To truly understand and optimize the performance of catalyst pellets, *operando* measurements of the concentration profile within industrially relevant catalyst pellets are needed.

The objective of this work is to develop and apply a magnetic resonance method to achieve the *operando* measurement of intra-pellet composition at the pellet scale. An introduction to the current understanding of concentration profiles within catalyst pellets is given, and the experimental measurement of intra-pellet concentration is subsequently reviewed. In this work, styrene hydrogenation over a Pd/Al_2O_3 catalyst is studied using magnetic resonance spectroscopic imaging (MRSI). In particular, the case of asymmetric wetting of the pellet surface is considered, typical of the situation found in trickle-bed reactors. Slice-selective spectroscopic MRI is implemented with compressed sensing to enable the acquisition of

quantitative two-dimensional (2D) maps of the concentration profile within operating catalyst pellets at an in-plane resolution of 86 μm. The resulting images reveal that partial wetting of the catalyst pellet significantly influences the intra-pellet composition profile. Due to the highly asymmetric wetting and mass transport boundary conditions at the pellet surface, commonly applied one-dimensional (1D) models are found to be inadequate to describe the composition profile at the pellet-scale. The measurements reported in this work give the first direct experimental insight into the effect of partial wetting on the concentration profile within an operating catalyst pellet. Further, the operando method developed can be used to investigate the complex coupling between the pellet-scale wetting, transport, and reaction within an operating reactor with the goal of ultimately optimizing the wetting and mass transport properties of industrially-relevant catalyst pellets.

1.1 Concentration profile within a catalyst pellet

The concentration profile within a catalyst pellet is described by the steady-state reaction-diffusion equation, with appropriate boundary conditions at the pellet surface to describe the external mass transport. For an isothermal, irreversible first-order reaction A → B, the steady-state reaction-diffusion equation is written [12,13]:

$$D\nabla^2 C_\mathrm{A} = kC_\mathrm{A}\,, \tag{1}$$

where ∇^2 is the Laplace operator, D is the intra-pellet diffusivity of A, C_A is the concentration of A, and k is the kinetic rate constant for the first order reaction. In dimensionless form, Equation (1) is written:

$$\nabla^2 c_\mathrm{A} = \Phi^2 c_\mathrm{A}\,, \tag{2}$$

where c_A is the dimensionless concentration of A normalized by the average concentration at the pellet surface ($c_\mathrm{A} = C_\mathrm{A}/C_\mathrm{A,s}$) and Φ is the Thiele modulus defined as $\Phi = r_\mathrm{p}\sqrt{k/D}$ and r_p is the pellet radius. Note that here it is assumed that the diffusivity, D, is independent of composition. Analytical solutions to Equation (2) exist only for simple geometries and boundary conditions. For the case of a spherical pellet with uniform surface concentration, $c_\mathrm{A}(r/r_\mathrm{p} = 1) = 1$, and finite concentration at the pellet centre, $c_\mathrm{A}(r/r_\mathrm{p} = 0) = \mathrm{constant}$, the analytical solution to Equation (2) is written as [13]:

$$C_{\mathrm{A}}(r) = C_{\mathrm{A,s}} \frac{r_{\mathrm{p}} \sinh\left(\frac{\Phi r}{r_{\mathrm{p}}}\right)}{r \sinh(\Phi)} \,. \tag{3}$$

For the case where only species A and B are in solution, if C_{A} is written in units of mole fraction, then the concentration of product is simply given as $C_{\mathrm{B}} = 1 - C_{\mathrm{A}}$. The concentration of product and reactant computed from Equation (3) for two different values of the Thiele modulus is shown in Figure 1. Clearly, the concentration of reactant, C_{A}, decreases monotonically towards the centre of the pellet and the concentration of product, C_{B}, increases monotonically from the pellet surface to centre. This occurs because of the balance between the rate of diffusion and reaction at steady state (Equation (1)), and the uniformity of the boundary conditions imposed. Further, the ratio of the rate of reaction to diffusion, as quantified by the Thiele modulus, Φ, markedly influences the distribution of product and reactant throughout the pellet.

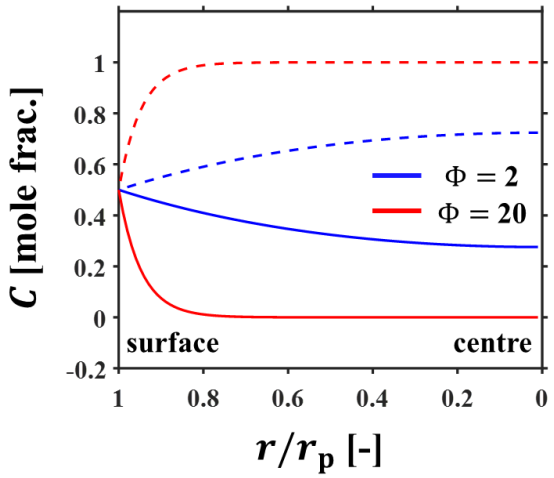

Figure 1. Concentration profile for a first order isothermal reaction in a spherical catalyst pellet with uniform boundary conditions, computed using Equation (*3*) for two values of the Thiele modulus, Φ using an arbiraty value of the surface concentration $C_{\mathrm{A.s}} = 0.5$. Solid lines represent the concentration of reactant, C_{A}, whilst dashed lines represent the concentration of product, C_{B}. The surface and centre of the pellet are identified as $r/r_{\mathrm{p}} = 1$ and $r/r_{\mathrm{p}} = 0$, respectively.

In trickle beds, non-uniform (partial) wetting is well-known to occur, whereby the catalyst pellet is only partially covered with liquid [14,15]. As a result, the mass transport at the pellet surface is highly non-uniform, and uniform boundary conditions cannot be used to describe the mass transport. Therefore, to model the intra-pellet concentration profile, Equation (2) must be numerically solved, considering the partial wetting of the catalyst pellet. Tang *et al.* [16] recently studied the effect of partial wetting on the concentration profile within catalyst pellets by numerically solving Equation (2) for physically realistic wetting geometries using

the finite element method (FEM). The results reported by Tang *et al.* clearly demonstrated that asymmetric partial wetting of a catalyst pellet resulted in highly asymmetric intra-pellet concentration profiles for mass transport limited conditions; both liquid-species limiting and gas-species limiting conditions were considered.

To date, asymmetry in concentration within a pellet in a trickle bed has not been directly observed experimentally, in large part due to the lack of techniques capable of measuring concentration within heterogeneous catalysts. The variation of concentration within a pellet will obviously influence the rate of reaction within the pellet. In reactor modelling, this is accounted for through the effectiveness factor, which describes the average intra-pellet rate of reaction relative to the reaction rate at the pellet surface [13]. Significant efforts have been made to develop general correlations for the effectiveness factor of partially wetted catalysts [16–19]. However, these models remain unvalidated by experimental measurements, and their validity for describing the reaction-diffusion dynamics in real pellets remains unknown. Hence, directly measuring the concentration profile within an operating pellet at high resolution is of great interest to further understand the complex reaction-diffusion phenomena occurring within working catalyst pellets.

1.2 Operando measurements of intra-pellet concentration in packed bed reactors

Experimental spatially-resolved measurements of the composition within catalyst pellets with which reaction-diffusion models can be validated and calibrated are extremely scarce in the literature. Whilst *operando* methods used in the catalysis community [1,20] have become greatly sophisticated for investigation at the nano- and micro-scale, measurements of composition at industrially relevant length-scales such as the pellet-scale are in their infancy. Indeed, considering the ubiquity of heterogeneous catalysts in industry, there are remarkably few spatially-resolved measurements of intra-pellet composition reported in the literature. Chmelik *et al.* [21] used infrared microimaging to acquire 2D images of the intra-pellet composition during benzene hydrogenation to cyclohexane over a Pt catalyst dispersed in a nanoporous glass pellet, achieving an in-plane spatial resolution of 3 μm × 3 μm; the imaging slice thickness or penetration depth of the infrared in this study was not given. Despite the impressive resolution achieved in this study [21], the spatially-resolved measurements were only reported to be semi-quantitative, and the infrared method cannot be used on optically-opaque supports that are frequently used in commercial processes. Sosna *et al.* [22] designed

a novel capillary sampling method whereby a channel is drilled within a catalyst pellet and a microcapillary is inserted within the channel, thus enabling the composition to be sampled from various points within the pellet during operation, achieving a spatial resolution of ~100 μm. Great care was taken to ensure the design of the channel and micro-capillary did not appreciable alter the flow in the reactor or the reaction-diffusion processes occurring within the pellet. The results demonstrated the complex interaction between reaction and diffusion within a pellet, with phenomena such as multiple steady states and kinetic oscillations being observed. However, it would be difficult to obtain information in more than one dimension using this capillary method, and further in a trickle bed the capillary would likely interfere with the pellet wetting.

Due to its inherently quantitative nature, and its applicability to optically opaque systems, magnetic resonance methods are perhaps uniquely capable of making *operando* measurements of intra-pellet composition at commercially-relevant length scales. The use of MRI for studying catalysts and catalytic processes has been reviewed by Gladden and co-workers [3,23,24], and a recent review from Pesch *et al.* [5] discusses the use of *operando* MRI for studying multiphase catalytic reactors. Several studies have used 1D magnetic resonance spectroscopic imaging (MRSI, also known as chemical shift imaging (CSI) to study the chemical conversion along the length of catalytic reactors for various reactions, including an esterification reaction over an ion exchange resin [25,26], and the hydrogenation of 1-octene [9,10], hydrogenation of 1,3-butadiene [27] and oligomerization of ethene [11] over supported metal catalysts. Many of these studies were able to obtain the intra- and inter-pellet composition by using relaxation or diffusion weighting during the acquisition of spectra, or by conducting partial least squares regression on the acquired spectra. Whilst such 1D information can be used to understand the behaviour of reactors at *operando* conditions and validate reactor models, the 1D measurements are insufficient for studying the reaction and transport at the pellet-scale. MRSI has previously been used to acquire 2D and 3D images of the chemical composition during an esterification reaction in a bed of ion exchange resin pellets at a resolution ~ 600-700 μm [23,26]. These studies observed remarkable heterogeneity in the composition within the reactor, and gave insight into the true rate limiting processes impacting reactor performance. However, the resolution still did not permit the investigation of the reactor at the pellet-scale as the pellets used were approximately the same size as the image resolution. Recently, Ulpts *et al.*[6,7,28] have used MRSI to obtain 2D and 3D chemical composition maps for the hydrogenation of ethene to

ethane over random and structured catalyst packings at a resolution of ~1 – 1.5 mm. These measurements of chemical composition were combined with NMR thermometry measurements, and subsequently compared to a 1D reactor model, showing good agreement between model and experiment. The formation and transport of species within an individual pellet at a resolution ~200 μm [29] and at the reactor-scale at a resolution ~1 mm [30] has been studied using MRI without spectroscopic resolution for gas-phase hydrogenation reactions, revealing heterogeneity in the accumulation of products within the intra-pellet space. Küppers *et al.* [31] used 1D-MRSI and 2D MRI (without spectroscopic resolution) at a resolution of ~80 μm to study the reaction-diffusion behaviour of an esterification reaction within a single hydrogel pellet. The reaction-diffusion behaviour was found to be significantly asymmetric across the pellet, which was attributed to structural heterogeneity within the pellet. Recently, Burueva *et al.* [32] mapped the relative concentration of propane and propene within a Pt/Al_2O_3 pellet during the hydrogenation of propene at a resolution of ~ 200 μm; the observed conversion was observed to be 100%, showing little heterogeneity. Finally, Zheng *et al.* [4] used 2D diffusion MRI to map the carbon number distribution during Fischer-Tropsch reaction over a Ru/Ti_2O_3 catalyst at an in-plane spatial resolution of 200-300 μm. Significant composition heterogeneity was observed at both the pellet- and bed-scale, attributed to local mass transfer limitations in the bed due to the accumulation of heavy liquid products during the Fischer-Tropsch reaction.

From the above reviewed studies, it is clear that magnetic resonance offers a unique capability for measuring intra-pellet concentration at *operando* conditions in catalytic reactors. However, most measurements have been made at low resolution and few studies have utilized the capability of MRI to make measurements at the pellet-scale. Such measurements promise to give insight into the coupling between transport and reaction within a catalyst pellet at relevant operating and wetting conditions, and offer avenues towards optimizing the design of catalyst and reactor technologies. In this work, the chemical composition of intra-pellet liquid is mapped within a 3.2 mm diameter Pd/Al_2O_3 catalyst using 2D MRSI at an in-plane isotropic spatial resolution of 86 μm during the hydrogenation of styrene to ethylbenzene. The results demonstrate that inhomogeneous wetting causes significant composition heterogeneity at the pellet-scale.

2 Materials and methods

2.1 Materials and reaction

The reaction studied in this work was the hydrogenation of styrene to ethylbenzene over a Pd/Al_2O_3 catalyst. This reaction was selected for several reasons. First, styrene and ethylbenzene can be easily distinguished through their respective NMR spectra [33]. As shown in Section 3.1, the aliphatic hydrogens can easily be distinguished from the aromatic and olefinic hydrogens in the NMR spectra, even within a catalyst pellet where the NMR lineshape is significantly broadened, thus allowing the concentration of styrene and ethylbenzene to be obtained from the spectra. Second, due to the fast kinetics, this reaction is known to be limited by the rate of hydrogen mass transport, even at ambient conditions [34–36]. Studying a mass transfer limited reaction, as opposed to a reaction limited by the intrinsic reaction kinetics, allows for the coupling between diffusion, wetting and reaction to be investigated; importantly, the mass-transfer limited regime is applicable in many commercial trickle-bed processes [37]. Finally, this hydrogenation reaction serves as a model system for more complex hydrotreating and selective hydrogenation reactions that are encountered in the petrochemical and fine chemicals industries. However, in the context of the present work it is not the nature of this specific reaction that is of interest, but rather the ability to probe the reaction-diffusion behaviour at the pellet-scale within a working catalyst.

Styrene (>99% purity, Fisher Scientific) stabilized with 10 – 15 ppm 4-tert-butylcatechol (to prevent spontaneous polymerization of styrene) and hydrogen gas (99.99% purity, BOC) were used as feedstock for the reaction. Porous 1/8" (3.2 mm) diameter cylindrical alumina pellets (Alfa Aesar) with pore volume of 0.57 – 0.67 mL g^{-1} and specific surface area of 200 m^2 g^{-1} as measured by the supplier were used as the catalyst support. The alumina pellets were prepared using an incipient wetness impregnation with a $Pd(NH_3)_4(OH)_2$ solution to give a uniform metal loading of 0.5 wt%. After impregnation the catalysts were dried overnight at 120 °C and calcined for 2 h at 300 °C. Visual inspection of the catalysts showed an approximately uniform metal distribution throughout the pellet (Supplementary Information). Before loading the reactor, the pellets were dried for 16 h at 200 °C.

2.2 Reactor and experimental setup

The reactor and experimental setup used to conduct *operando* magnetic resonance measurements is shown in Figure 2. Viton™ fluoropolymer (Chemours) tubing of 5 mm inner diameter (ID) was used to facilitate the reaction, thus giving a tube-to-pellet diameter ratio of $N = 1.6$ for the reactor. Such a low aspect ratio makes this reactor a single-pellet-string-reactor (SPSR) [38]. Whilst beds of larger N are used in commercial trickle bed processes, SPSRs are useful for lab- and pilot-scale studies as the pellet-scale transport phenomena are similar to that in large reactors. Glass ballotini (diameter 3 mm) were loaded into the Viton™ tubing to a height of 30 mm, following which 4 Pd/Al_2O_3 pellets were randomly loaded into the tube. Another 30 mm layer of glass ballotini was placed on top of the catalyst pellets. The packing was supported by 5 mm of glass wool packed into the bottom of the tube. Following packing, the reactor was passed through the bore of the NMR spectrometer. Fluorinated ethylene propylene (FEP) tubing was used to facilitate the flow of reagents to and from the reactor. Hydrogen gas was introduced to the reactor at ~1.1 bar using a regulator valve and the flow rate was set manually using a variable area flow meter equipped with a needle valve. Liquid styrene flow was supplied using a HPLC pump (Agilent 1100 series). Liquid and gas feed were mixed in a T-joint and fed co-currently to the top of the reactor tubing. The amount of liquid in the bed was verified to be steady using a simple pulse-acquire NMR method, thereby confirming that the liquid flow was steady and not pulsing. Liquid product was allowed to accumulate in a 1 L glass Schott bottle fitted with a rubber septum with a vent line to allow H_2 to vent to atmosphere. Liquid product samples were periodically collected into an NMR tube for off-line analysis by opening the needle valve (9) in Figure 2.

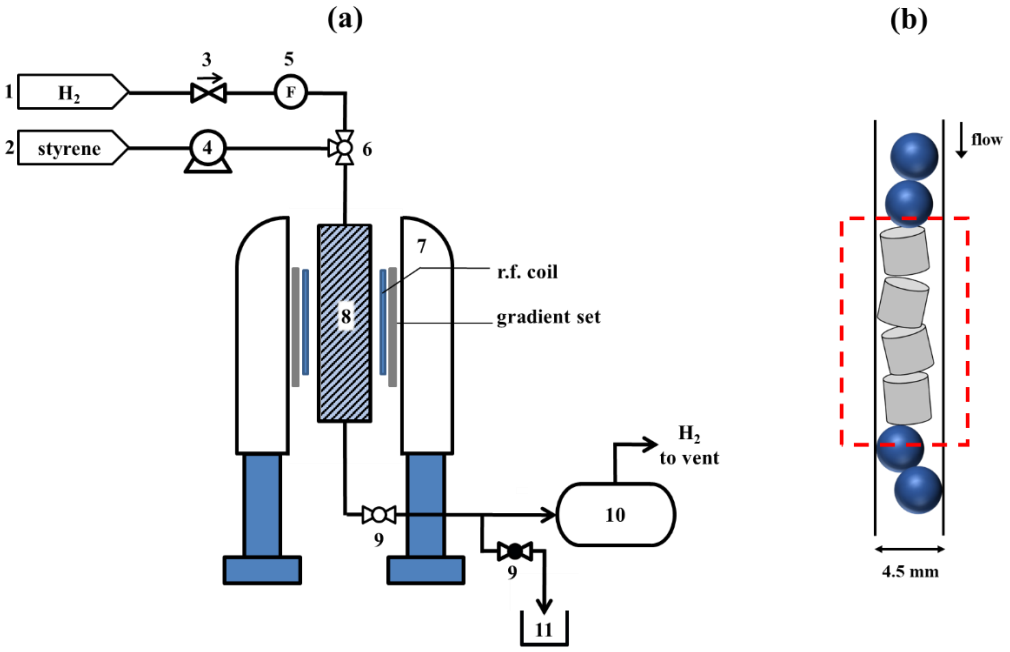

Figure 2. Schematic of reactor and experimental setup used to conduct *operando* magnetic resonance measurements. **(a)** Experimental setup: (1) H_2 gas supply, (2) liquid styrene supply, (3) regulator valve, (4) HPLC pump, (5) variable area flow meter with needle flow control valve, (6) three way T-joint, (7) 7.0 T superconducting magnet, (8) 5 mm ID Viton tubing used as reactor, (9) ball valve, (10) 1 L glass bottle with rubber septum for accumulation of liquid product and venting of H_2, (11) 250 mL glass Schott bottle for periodic liquid product collection. **(b)** Detailed schematic of reactor: grey cylinders represent catalyst pellets while blue spheres represent glass ballotini. The red dashed box represents the active region of the NMR probe.

2.3 Reactor operation

The reactor was packed and loaded into the NMR spectrometer as described in Section 2.2. The palladium catalyst was reduced by flowing hydrogen through the bed at a flow rate of 12 NL h^{-1} at ~1.1 bar for 2.5 h. Following reduction of the catalyst, the bed was purged with nitrogen gas for 1 h (note that the N_2 line is not shown in Figure 2, but ran parallel to the H_2 feed line). The bed was then flooded with pure styrene by connecting the reactor outlet to the pump and pumping styrene upwards into the bed. The pellets were allowed to saturate with styrene for 12 h, following which a reference image of the bed structure was taken (using 3D RARE imaging, as described in Section 2.4). The bed was then drained under gravity for 30 min. Liquid styrene and gaseous nitrogen flow were then introduced to the bed at a flow rate of 0.02 mL min^{-1} and 1.0 NL h^{-1}, respectively. The reaction was then started by turning off the N_2 gas flow and switching to H_2 gas feed at a flow rate of 3.0 NL h^{-1} whilst maintaining the styrene flow rate at 0.02 mL min^{-1}, thus corresponding to a molar feed ratio of ~ 10:1 H_2:styrene. The reaction was monitored by acquiring spatially-unresolved NMR spectra, and

also by collecting liquid product samples from the reactor. Once the reaction reached steady-state, 2D MRSI and 3D RARE imaging experiments (described in Section 2.4) were conducted to acquire images of the composition, and liquid distribution within the bed, respectively. During reactor operation, the reactor conversion was monitored as a function of time-on-stream (TOS) by periodically sampling the reactor effluent and (using valve (9) in Figure 2) and analysed offline using a benchtop NMR spectrometer (as described in Section 2.4). All experiments were conducted at approximately ambient pressure, and an external temperature of 20 °C.

All operando experiments reported in the main text were conducted using the above-mentioned conditions, notably a liquid styrene flow rate of $L = 0.02$ mL min^{-1}. Additionally, a preliminary investigation of the effect of liquid flow rate was conducted and is reported in the Supplementary Information. These experiments were performed following completion of experiments at the above-mentioned conditions. The liquid flow rate was then increased to $L = 0.2$ mL min^{-1}, and the same magnetic resonance experiments as used at the $L = 0.02$ mL min^{-1} condition were performed.

2.4 Magnetic resonance experiments

All NMR experiments were conducted using a vertical-bore 7.0 T superconducting magnet controlled by a Bruker BioSpin Avance III HD spectrometer. A 10 mm radiofrequency (r.f.) saddle coil tuned to a ^{1}H resonant frequency of 299.84 MHz was used for signal excitation and acquisition with a typical 90° hard pulse duration of 9.5 μs. A tri-axial gradient set (Bruker Micro5) with a maximum gradient strength of 2.9 T m^{-1} was used to achieve spatial resolution in three orthogonal directions. All chemical shift values are given with reference to the ^{1}H resonance of teramethylsilane (TMS).

Slice-selective MRSI [39] with spatial resolution in 2D was conducted using the pulse sequence shown in Figure 3. A 256 μs sinc-shaped soft 90° r.f. pulse (FWHM bandwidth of 8 kHz) was used for slice-selective signal excitation. The sinc shape was chosen to ensure uniform excitation of signal across the NMR spectra. To achieve slice-selective excitation, a gradient in the z-direction (axial) was applied during the excitation pulse, with the gradient magnitude calibrated to give a slice thickness of 2 mm. In contrast to 180° slice-selective pulses, 90° slice selection is not self-refocusing. To refocus the signal following slice selection, the slice gradient was applied with an equal magnitude in the opposite direction for a period of 300 μs (this duration was calibrated to give the maximum signal intensity upon

refocusing). A 19 μs rectangular hard 180° r.f. pulse was used for spin-echo refocusing. The resulting echo time was 650 μs. 2D spatial resolution was achieved using a phase-encode gradient pulse of 300 μs, stepped independently in the x and y directions. Images were acquired on a 64 (x) × 64 (y) raster with a FOV of 5.5 mm (x) × 5.5 mm (y), giving an in-plane isotropic resolution of 86 μm. For each excitation, signal was acquired by sampling 3k complex points using a spectral width of 10 kHz. Signal was averaged over 4 scans, and the repetition time was 2 s, giving a total acquisition time of 9 h for a fully sampled image. To accelerate image acquisition, compressed sensing was implemented at a sampling rate of 30%, thereby reducing the acquisition time to 3 h for compressed sensing acquisitions. The fidelity of the compressed sensing results is presented and discussed in the Supplementary Information.

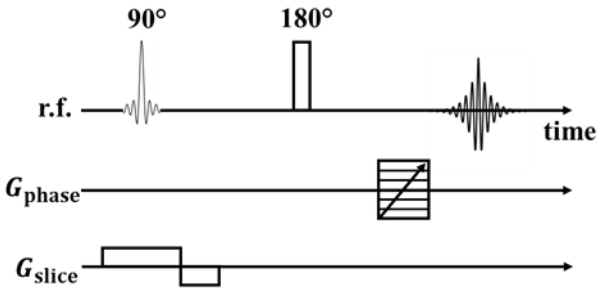

Figure 3. Pulse sequence used for 2D slice-selective MRSI.

To image the bed structure and the inter-pellet liquid distribution, 3D rapid acquisition with relaxation enhancement (RARE) imaging [40] was used. Hard rectangular 90° excitation and 180° refocusing pulses of duration 9.5 μs and 19 μs, respectively, were used. A RARE factor (number of lines of **k**-space acquired per excitation) of 64 was used with an inter-echo spacing of 1.4 ms. Images were acquired on a 64 (x) × 64 (y) × 256 (z) raster with a field-of-view (FOV) of 5.5 mm (x) × 5.5 mm (y) × 22 mm (z), giving an isotropic resolution of 86 μm. A repetition time of 7 s was used and 16 scans were collected for signal averaging, giving a total acquisition time of 2 h for a 3D image of ^{1}H spin density in the bed.

To measure the intra- and inter-pellet relaxation (both T_1 and T_2) and diffusion properties for both styrene and ethylbenzene, standard Carr-Purcell-Meiboom-Gill (CPMG) [41,42], inversion recovery, and alternating pulsed gradient stimulated echo (APGSTE) [43] pulse sequences, were used. For the T_2 measurements using CPMG, the echo time was 1 ms, the number of echoes was varied from 4 to 4096 in 8 uneven steps, the repetition time was 15 s, and 4 scans were conducted. For the T_1 measurements using inversion recovery, the variable

T_1 encoding delay was varied from 10 ms to 10 s in 12 unevenly spaced steps. Four scans were conducted with a repetition time of 15 s. For the diffusion measurements using APGSTE, a diffusion time of $\Delta = 30$ ms was used and gradient pulses of 0.5 ms duration were used to encode for diffusion, with a gradient stabilization delay of 0.3 ms. The gradient amplitude was varied from 0 to 1.5 T m^{-1} in 12 equally spaced steps. A repetition time of 15 s was used and 8 scans were collected.

To measure the reactor conversion, liquid product samples were collected periodically and analysed offline using a benchtop NMR spectrometer (Oxford Instruments Pulsar) equipped with a 1.4 T permanent magnet (^{1}H resonant frequency of 60 MHz). Liquid product was collected in a 4 mm NMR tube and spectra were acquired using a simple pulse-acquire sequence. A hard rectangular 90° pulse of duration 11.4 μs was used for signal excitation, and 8k complex points in the free induction decay were acquired at a spectral width of 50 kHz. The signal was averaged over 4 scans and a repetition time of 20 s was used to ensure complete signal recovery of all species within the reaction mixture.

2.5 Data processing and compressed sensing

Compressed sensing (CS) was implemented to accelerate data acquisition for the 2D MRSI experiments. Only 30% of **k**-space was sampled, using a sampling scheme that was generated using the method of Karlsons *et al.* [44]. Note that the spectral domain was fully sampled. The images were then reconstructed by solving an appropriately formulated inverse problem [45] using the object oriented mathematics for inverse problems toolbox developed by Benning [46] using total variation (TV) regularization with a regularization parameter of $\alpha = 0.01$ and 3 Bregman iterations, both of which were selected heuristically. Prior to reconstruction, a sine apodization function was applied in both directions of **k**-space. Note that since both the spectral and **k**-space dimensions are acquired in Fourier space, the full 3D dataset was reconstructed and inverted jointly, in a manner similar to that employed by de Kort *et al.* [47] for reconstructing maps of the displacement propagator. Following reconstruction, the resulting spectra from each voxel were automatically 0^{th} and 1^{st} order phase corrected by minimizing the sum of squares of the real portion of the tails of the spectra (where no signal is expected). After phase correction, the spectra from each voxel were automatically baseline corrected by fitting a 2^{nd} degree polynomial to both tails of the spectra. The resulting 2D MRSI dataset, consisting of two spatial dimensions and one

spectral dimension, could then be used to obtain a composition map, as presented in Section 3.1.

The data acquired from 3D RARE imaging experiments were processed by Fourier transforming the data in all three dimensions. The resulting 3D image of ^{1}H spin density were then segmented using Otsu's method [48]. The RARE acquisition was sufficiently T_2 weighted such that minimal signal was observed from intra-pellet fluid. Thus, the segmented images gave a map of the inter-pellet liquid within the reactor. The 3D image acquired for the fully-flooded bed was used to generate a map of the catalyst pellets within the bed, and the 3D images acquired at *operando* reaction conditions were used to map the inter-pellet liquid within the bed during the reaction.

2.6 Reference sample used to evaluate quantitative nature of MRSI measurements

To evaluate the quantitative nature of the CS MRSI implemented here, a reference sample of known composition was used to test the MRSI sequence and evaluate the resulting measured composition. A 4 mm NMR tube containing ethylbenzene was placed inside a 10 mm NMR tube containing styrene. Both tubes also contained the catalyst pellets used during the hydrogenation reaction. 2D MRSI experiments were conducted with full sampling of **k**-space, and the resulting data were numerically undersampled to evaluate the effect of CS on the measurement of composition, as described in the Supplementary Information. All imaging parameters were identical to those given in Section 2.4, except the FOV which was enlarged to 10 mm × 10 mm.

The results of the testing on this reference sample are presented in Section 3.1, and a further analysis of the effect of CS is reported in the Supplementary Information. In summary, the CS MRSI technique implemented in this work yields measurements of the intra-pellet concentration with a root mean squared error (RMSE) of ± 0.041 (mole fraction). Therefore, the intra-pellet composition measurements reported in this work can be interpreted quantitatively with a high degree of accuracy.

3 Results and discussion

3.1 Quantitative imaging of composition at the pellet-scale: evaluation using a reference sample of known composition

The MRSI results for the reference sample consisting of a tube of ethylbenzene within a tube of styrene (described in Section 2.6) are shown in Figure 4. From the image of signal intensity shown in Figure 4a, each tube is clearly seen, and the catalyst pellet within each tube can be seen from the circular region of decreased signal intensity. The voxels denoted p1 and p2 contain inter-pellet styrene and ethylbenzene, respectively, and the spectra from these voxels are shown in Figure 4c and d, respectively. These are consistent with the known NMR spectra for both species [33]. For the styrene, the peak at ~7.7 ppm corresponds to aromatic hydrogen, whilst the peaks at ~6.7, 5.7, and 5.2 ppm correspond to olefinic hydrogens. For the ethylbenzene, the peak at ~7 ppm similarly corresponds to aromatic hydrogens, while the peaks at ~1 ppm and ~3 ppm both correspond to aliphatic hydrogens. The voxels denoted p3 and p4 contain intra-pellet styrene and ethylbenzene, respectively, with the respective spectra shown in Figure 4e and f. Significant line-broadening is observed for the intra-pellet spectra, due to magnetic susceptibility differences within the pellet causing internal magnetic field gradients. However, the distinctive shift of the aliphatic peaks of the NMR spectra (1 – 3 ppm) compared to the olefinic and aromatic peaks (5 – 7 ppm) allows for the quantification of composition from the NMR spectra. Considering that there are 5 aliphatic hydrogens per molecule of ethylbenzene, the magnitude of the aliphatic peaks in the NMR spectra, I_{al}, is written as:

$$I_{\mathrm{al}} = 5\lambda n x_{\mathrm{EB}} \,, \tag{4}$$

where n is the number of molecules within the voxel and λ is the response factor of the spectrometer (an empirical proportionality term describing the signal contribution per spin). Similarly, because there are 5 aromatic hydrogens in both ethylbenzene and styrene and further 3 olefinic hydrogens in styrene, the magnitude of the combined aromatic and olefinic peaks in the NMR spectra, $I_{\mathrm{ar,ol}}$, is written as:

$$I_{\mathrm{ar,ol}} = 5\lambda n x_{\mathrm{EB}} + 8\lambda n(1 - x_{\mathrm{EB}}) \,. \tag{5}$$

By combining Equations (4) and (5), the fraction of signal from the aliphatic peaks, f_{al}, is written:

$$f_{al} = \frac{I_{\mathrm{al}}}{I_{\mathrm{al}} + I_{\mathrm{ar,ol}}} = \frac{5x_{\mathrm{EB}}}{8 + 2x_{\mathrm{EB}}}. \quad (6)$$

By rearranging Equation (6), the mole fraction of ethylbenzene, x_{EB}, is written as:

$$x_{\mathrm{EB}} = \frac{8f_{\mathrm{al}}}{5 - 2f_{\mathrm{al}}}. \quad (7)$$

Thus, for a binary mixture of ethylbenzene and styrene, the composition can be quantified directly from the fraction of the spectral intensity in the aliphatic region (located at 1 – 3 ppm). The composition map for the reference sample, calculated from the spectra in each voxel from the 2D MRSI data using Equation (7), is shown in Figure 4b. A chemical shift of ~4.5 ppm was used as the cut-off to demarcate the aliphatic region from the olefinic and aromatic region of the spectra. The composition map in Figure 4b clearly shows the true composition of the reference sample, with a root mean square error (RMSE) of 4.1% (mol fraction), and demonstrates that the 2D slice-selective MRSI sequence can be used to map the composition of the reference sample both within and outside the catalyst pellet. For binary mixtures of ethylbenzene and styrene, it is important to consider the potential for relaxation and diffusion weighting of the spectra which could make the results non-quantitative. The relaxation and diffusion properties of styrene and ethylbenzene, measured as described in Section 2.4, are reported in the Supplementary Information. The intra-pellet relaxation and diffusion are similar for both styrene and ethylbenzene, and thus quantitative measurement of intra-pellet composition for binary mixtures will not be hindered by either relaxation or diffusion weighting. However, for the bulk (inter-pellet) fluid, the relaxation and diffusion properties differ between ethylbenzene and styrene. Given the short echo time used in the pulse sequence, the differences in T_2 will not result in any relaxation weighting of the spectra. However, the differences in T_1 may lead to significant relaxation weighting considering the repetition time used is only 2 s. To achieve quantitative measurements of inter-pellet composition, in future implementations of this work, the repetition time may be increased to remove T_1 weighting (at the expense of longer data acquisition times), or a correction scheme for T_1 weighting may be applied. Due to the differences in inter-pellet T_1, and the short repetition time used in this work, the inter-pellet composition measured during the reaction can only be interpreted qualitatively. However, the intra-pellet measurement of composition can be interpreted quantitatively.

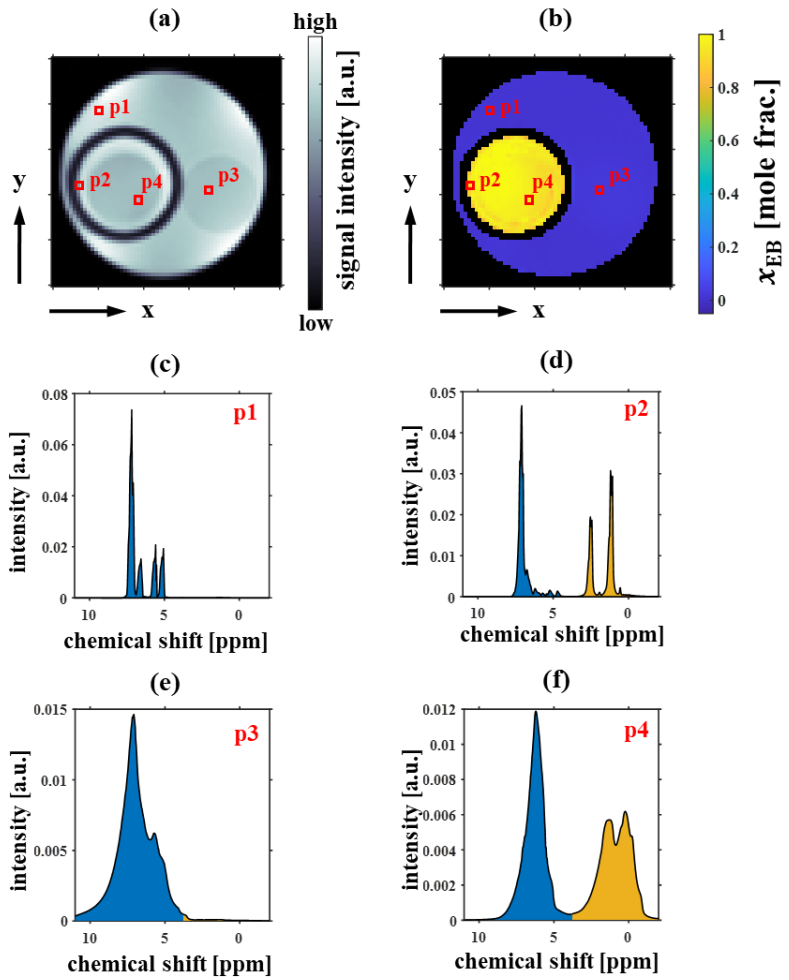

Figure 4. (a) Fully sampled 2D MRSI image of reference sample consisting of 4 mm tube of ethylbenzene within a 10 mm tube of styrene, both tubes containing catalyst pellets. ^{1}H signal density image obtained by summing entire spectra in each voxel; (b) composition map showing mole fraction of ethylbenzene, x_{EB}, obtained from the 2D MRSI dataset using Equation (7). Images shown have a FOV of 10 mm (x) × 10 mm (y) and an in-plane spatial resolution of 156 μm; (c) ^{1}H NMR spectra from voxel denoted p1 containing inter-pellet styrene; (d) ^{1}H NMR spectra from voxel denoted p2 containing inter-pellet ethylbenzene; (e) ^{1}H NMR spectra from voxel denoted p3 containing intra-pellet styrene; (f) ^{1}H NMR spectra from voxel denoted p4 containing intra-pellet ethylbenzene. In (c-f), blue shading represents the aromatic and olefinic peaks, while the yellow shading represents aliphatic peaks. Note that the four high signal intensity regions near the tube edge in (a) are caused by inhomogeneity in the B_1 (r.f.) field produced near the edges of the saddle coil.

3.2 *Operando* imaging of composition at the pellet-scale

The bed structure, and inter-pellet fluid in the reactor during operation at steady state operation is shown in Figure 5a. Note that successive repeat 3D images of the inter-pellet liquid revealed the liquid structure to be stable, with very minimal change observed for images taken 10 h apart (not shown). From Figure 5a, it is seen that the catalyst pellets are aligned nearly vertically in an ordered fashion. This is due to the low tube-to-pellet-diameter

ratio, $N = 1.6$, for this single pellet string reactor. The inter-pellet liquid in the bed is seen to partially wet the surface of the catalyst pellet, which is well known for both single pellet string reactors [49] and commercial-scale trickle bed reactors [15]. The clear wetting inhomogeneity at the pellet-scale presents an excellent opportunity in this study for evaluating how wetting inhomogeneity at the pellet-scale impacts composition and reaction heterogeneity at the pellet-scale.

Figure 5b-c shows a ^{1}H NMR intensity image for pellet 4, along with a concentration map of ethylbenzene for the same location in the bed, acquired using slice-selective 2D MRSI. The concentration map was calculated from the spectra measured within each voxel from the 2D MRSI data using Equation (7). Clearly, from the intensity image in Figure 5b, the catalyst pellet is partially covered in liquid, with the remainder of the pellet directly exposed to hydrogen gas. This results in significant composition heterogeneity across the pellet, as seen in Figure 5c. The side of the pellet that is directly exposed to hydrogen has substantially higher ethylbenzene concentration, $x_{\mathrm{EB}} \approx 0.2$, compared to the side of the pellet that is liquid-wet where $x_{\mathrm{EB}} \approx 0.05$. As previously mentioned, due to the differences in T_1 for inter-pellet styrene and ethylbenzene, the inter-pellet composition values cannot be interpreted quantitatively. However, the intra-pellet composition values can be interpreted quantitatively given that the relaxation and diffusion properties for intra-pellet styrene and ethylbenzene are nearly equal (Supplementary Information).

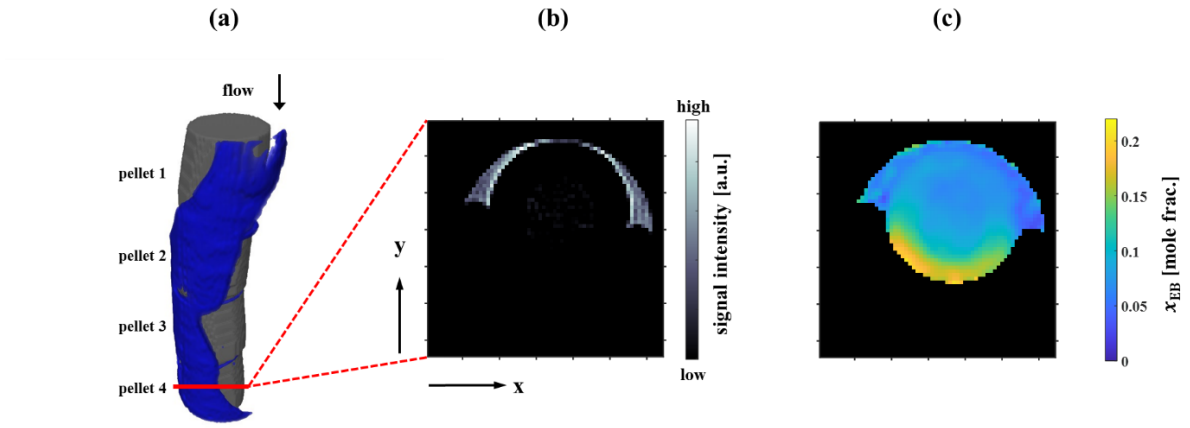

Figure 5. Reactor structure, liquid distribution, and resulting composition map. (a) Reactor structure and inter-pellet liquid as measured using 3D RARE MRI. Gray shading represents catalyst pellets and blue shading represents liquid flowing over the catalyst. Image was rendered using Avizo-Amira (Thermo-Fisher Scientific). The image of inter-pellet liquid was acquired at TOS = 30 h, whilst the location of the catalyst pellets was determined from the image acquired from the fully flooded bed, as described in Section 2.5. (b) 2D slice of 3D ^{1}H signal intensity image acquired using RARE MRI at TOS = 30 h. (c) Image of ethylbenzene concentration, x_{EB}, at TOS = 38 h as calculated from 2D MRSI acquisition using Equation (7). Images shown have a FOV of 5.5 mm (x) × 5.5 mm (y) and an isotropic in-plane spatial resolution of 86 µm. The slice thickness is 2 mm for the composition map shown in (c), while the image shown in (b) has a resolution of 86 µm in the direction into the page.

A more detailed investigation into the composition map shown in Figure 5 is given in Figure 6. The same composition map as that shown in Figure 5c is shown in Figure 6a but the voxels containing inter-pellet liquid have been shaded grey in order to clearly outline the pellet, and the location of the liquid wetting at the pellet surface. Further, the spectra from selected voxels across the pellet are shown in Figure 6b-d. Voxel p1, located in the centre of the pellet, contains a low concentration of ethylbenzene, $x_{\mathrm{EB}} \approx 0.07$, reflected by the corresponding spectra in Figure 6b which contains only very small aliphatic peaks. Moving outward towards the pellet surface exposed to gas, the concentration of ethylbenzene increases, as reflected by the spectra in voxels p2 and p3 which have increasingly larger aliphatic peaks as seen in Figure 6c,d.

The composition maps and spectra in Figure 5 and Figure 6 give clear evidence of the coupling between transport and reaction on the pellet-scale. In this gas-limited reaction, the reaction readily proceeds on the side of the pellet directly exposed to hydrogen. However, on the gas exposed side the ethylbenzene produced can only be removed by evaporation, which due to the low vapor pressure is very limited. As a result, to leave the pellet the ethylbenzene accumulates on the gas-exposed side and diffuses towards the liquid-wet side, causing a

concentration gradient across the entire pellet. This interpretation corresponds well with the simulations conducted by Tang *et al.* [16] for a gas-limited reaction.

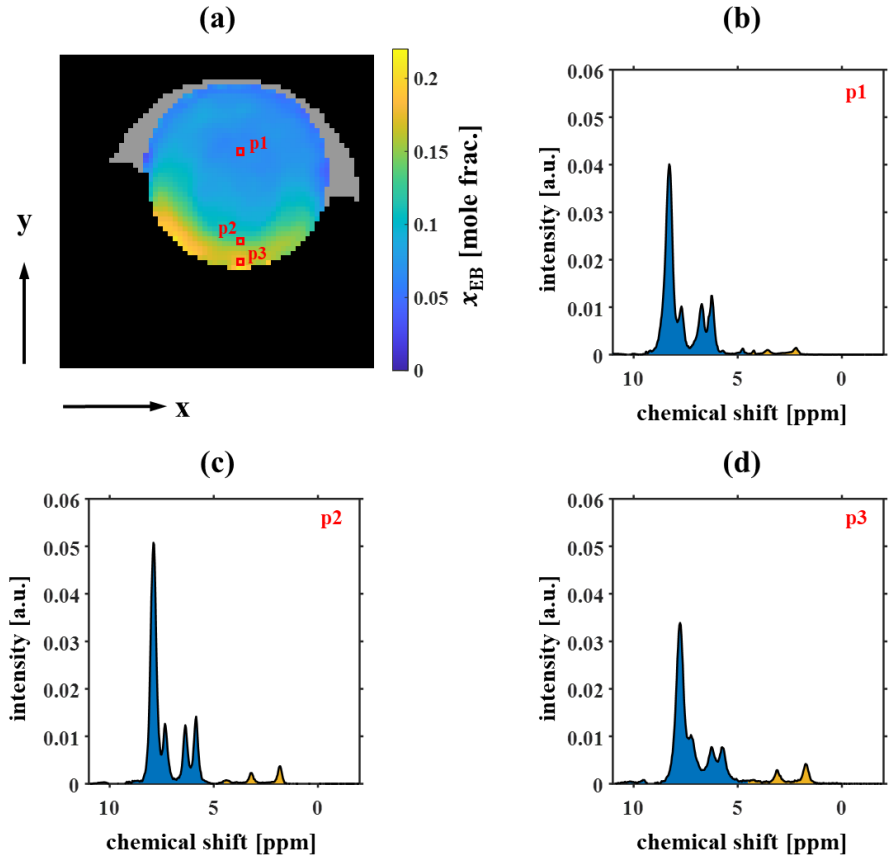

Figure 6. MRSI results for catalyst pellet 4. (a) image of ethylbenzene concentration, x_{EB}, at TOS = 38 h as calculated from 2D MRSI acquisition using Equation (7). The image has a FOV of 5.5 mm (x) × 5.5 mm (y) and an in-plane spatial resolution of 86 μm. Gray shading represents voxels containing inter-pellet liquid. (b) spectra from voxel p1; (c) spectra from voxel p2; (d) spectra from voxel p3. In the spectra shown in (b)-(d), blue shading represents the aromatic and olefinic peaks, while the yellow shading represents aliphatic peaks.

To further investigate the pellet-scale composition, composition maps obtained for pellets 2 and 4 at different TOS are shown in Figure 7. Further, composition maps obtained for pellet 2 and 4 at an increased liquid flow rate ($L = 0.2$ mL min^{-1}) are reported in the Supplementary Information. In all cases, irrespective of the pellet, TOS, or flow rate, the composition maps show a clear coupling with the pellet wetting. As previously described, the ethylbenzene concentration is highest at the gas-exposed side of the pellet, and decreases across the pellet to the liquid-wet side. The close similarity of the images acquired for pellet 4 at TOS = 38 h and TOS = 47 h confirms that the concentration gradient across the pellet is not merely a transient effect. The location of the pellet wetting for pellet 2 and 4 is significantly different, and the resulting concentration map shifts accordingly, as shown in Figure 7. Overall, all of the pellet composition maps acquired in this work agree with the previously discussed

interpretation, whereby the reaction proceeds readily at the gas-exposed surface, ethylbenzene accumulates and subsequently diffuses towards the inter-pellet liquid where it can be transported out of the reactor. These images of composition at the pellet-scale differ strongly with simple 1D reaction-diffusion models that predict the composition of product to decrease monotonically from the pellet centre to the surface. The reality for a partially-wetted pellet appears to be much more complex, as shown in Figure 7.

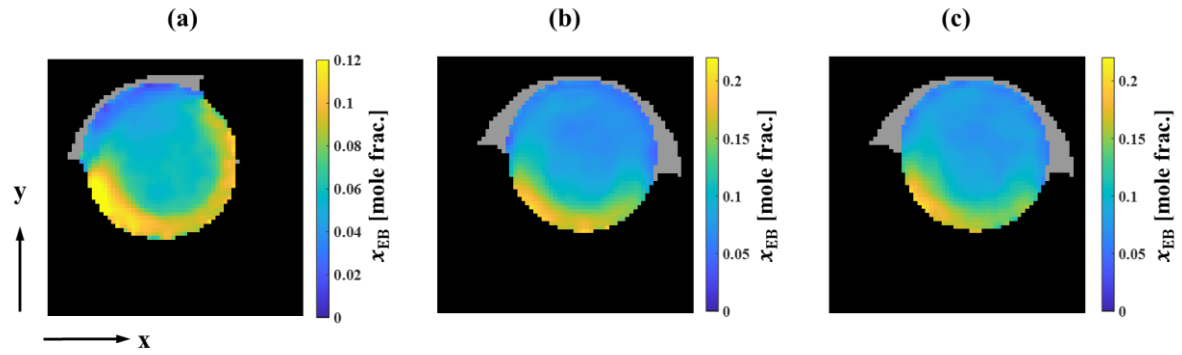

Figure 7. Pellet-scale images of ethylbenzene concentration, x_{EB}, during reactor operation. (a) pellet 2, acquired at TOS = 35 h; (b) pellet 4, acquired at TOS = 38 h; (c) pellet 4, acquired at TOS = 47 h. Images shown have a slice thickness of 2 mm, a FOV of 5.5 mm (x) × 5.5 mm (y) and an in-plane spatial resolution of 86 μm. Gray shading represents voxels containing inter-pellet liquid.

3.3 Radial profile of ethylbenzene concentration

The centreline concentration profile, along with the average radial concentration profile, for pellet 4 is shown in Figure 8. Figure 8b shows the concentration profile across the centreline (from the gas-exposed side to the liquid-wet side), as taken from the region indicated by the red line in Figure 8a. As shown in the composition profile, Figure 8b, the ethylbenzene concentration decreases significantly from the gas-exposed side to the liquid-wet side of the pellet. The centreline composition profile across the pellet (Figure 8b) closely resembles the concentration profiles from the numerical simulations of Tang *et al.* [16] which show the concentration of limiting reactant across partially wetted pellets.

The average radial profile, shown in Figure 8c, was calculated by azimuthally averaging the composition data shown in Figure 8a, thus giving the average composition as a function of distance from the pellet centre, r. The radial profile in Figure 8c shows the average ethylbenzene concentration increasing moving outwards from the pellet centre, followed by a small decrease near the pellet surface. The shaded region in Figure 8c, representing the

standard deviation of composition at a given radial position, shows that the heterogeneity in composition across the pellet increases towards the pellet surface, which is also visually reflected in Figure 8a. This heterogeneity in composition, as seen in the composition maps, cannot be adequately captured in 1D models which simply use a mean radial concentration profile. Clearly, the azimuthal averaging process to obtain an average radial profile results in a loss of information on the pellet-scale heterogeneity caused by asymmetric partial wetting.

The centreline and radial concentration profiles shown in Figure 8b-c, stand in stark contrast to the predictions for simple 1D radial reaction-diffusion models (Figure 1). The extensively utilized 1D reaction-diffusion model predicts the product concentration to decrease monotonically from the pellet centre to surface, whereas some of the *operando* measured profiles show an increase from the pellet centre. Further, it is interesting that the radial profiles for both pellets are observed to change significantly with liquid flow rate (Supplementary Information). This changing shape of the concentration profile implies that the apparent catalyst effectiveness factor changes with liquid flow rate, a result which cannot be predicted from simple 1D models. The *operando* composition images, and the radial profiles, provide direct experimental evidence of the coupling between wetting, transport, and reaction at the pellet-scale. Because of this coupling, and the wetting inhomogeneity observed at the pellet-scale, simple 1D models are inadequate to accurately describe the reaction-diffusion process occurring within the pellets. Simulations of reaction-diffusion within partially wetted pellets conducted by Bazer-Bachi *et al.* [17] demonstrated that 1D models are insufficient to model catalyst pellets when the mass and heat transport boundary conditions were highly asymmetric. This is an important finding as it suggests that more refined pellet-scale models are needed to describe reaction and transport at the pellet-scale in trickle beds compared to the 1D models that are commonly used. Mills and Dudukovic [12] developed a dual-series solution to compute the effectiveness factor of partially wetted pellets for precisely defined wetting geometries. In the limit of high Thiele modulus, the effectiveness factor of a partially wetted pellet was shown to be closely approximated by the effectiveness factor of a fully wetted pellet multiplied by the wetting fraction. However, as discussed by Mills and Dudukovic [12], use of this approximation outside the asymptotic range leads to significant underestimation of the true effectiveness factor. The single pellet simulations conducted by Tang *et al.* [16] showed that for a gas-limited reaction, the effectiveness factor could be modified for trickle beds by the modification proposed by Ramachandran and Smith [19] where the effectiveness factor for a partially-wetted pellet is taken as the weighted

average of the Thiele modulus contributions for a dry pellet and a fully wetted pellet. However, this modification assumes that wetted and dry areas of the pellet do not interact significantly, and Tang *et al.* [16] only tested this modification method for relatively high rates of external mass transfer. For general cases when the wetting is highly asymmetric and significant external transport limitations exist, it is possible that these simplified modification methods break down. In addition to mass transport heterogeneities, in the case of highly exothermic reactions, partial wetting may lead to significant heterogeneities in heat transfer, and the formation of local hot spots within a pellet.

The MRSI measurements reported here demonstrate that the pellet-scale composition profiles cannot be predicted by 1D (radially symmetric) models when the pellet wetting, and thus mass transport at the surface, is highly asymmetric. A similar conclusion was drawn by Bazer-Bachi *et al.* [17] from the results of numerical simulations of composition at the single pellet scale.

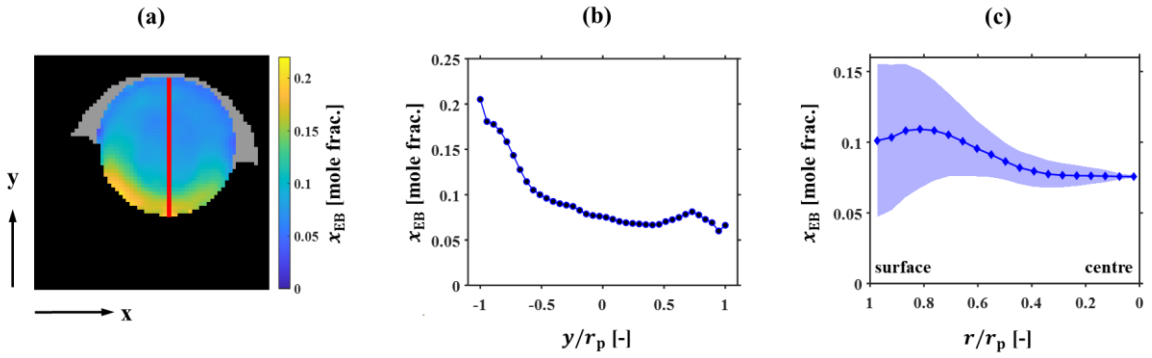

Figure 8. Ethylbenzene concentration profile, x_{EB}, across catalyst pellet 4 acquired at TOS = 38 h. (a) Ethylbenzene concentration map (identical to that reported in Figure 6). Note that the absolute uncertainty of the measurement of composition in each voxel is taken as $\pm$4.1% (mol frac.), as determined from the testing on the reference sample. (b) Centreline concentration profile across the catalyst pellet, from the region denoted by the solid red line in (a) going from the gas exposed side to the liquid-wet side. Concentration is plotted as a function of normalized distance along the y-axis from the centre of the pellet, y/r_p. (c) Radial profile of ethylbenzene concentration as a function of distance from pellet centre. The plotted line and symbols represent the mean concentration profile, while the shaded region represents one standard deviation of all concentration values at a given radial position within the pellet.

4 Conclusions

In this work, magnetic resonance methods were implemented to achieve the *operando* measurement of composition at the pellet-scale during the catalytic hydrogenation of styrene over a Pd/Al_2O_3 catalyst. A slice-selective 2D magnetic resonance spectroscopic imaging

pulse sequence was used to make spatially resolved spectroscopic measurements. Due to the distinct location of the aliphatic hydrogens in the NMR spectra, the concentration of ethylbenzene is quantified from the NMR spectra in each voxel, thus obtaining an image of liquid composition within the catalyst pellet. The 2D composition mapping was tested on a reference sample of known composition, achieving a root mean square error of 4.1%.

The pellet-scale intra-pellet composition maps acquired at an in-plane resolution of 86 μm during *operando* styrene hydrogenation reveal the direct coupling between wetting, mass transport, and reaction. The concentration of ethylbenzene within the pellet was found to be closely coupled to the wetting of the pellet surface, whereby the concentration decreased across the pellet from the gas-exposed surface to the liquid-wet surface, regardless of the pellet, liquid flow rate, or time-on-stream. The resulting radial profile of average concentration was found to be inconsistent with the prediction of simple 1D reaction-diffusion models, in agreement with simulations reported in literature. The results reported here provide unique experimental insight into the complexity of reaction-diffusion phenomena at the pellet-scale within an operating reactor. The magnetic resonance methods implemented here, and the resulting insight provided, have the potential to aid in the further optimization of the wetting and transport properties of commercial catalyst pellets. In particular, this approach enables us to gain insight to heterogeneities in pellet-scale mass transport and reaction for heterogeneously catalysed reactions; these data will aid the development and validation of improved reaction-diffusion modelling techniques for the case of partial catalyst wetting. A natural extension of this work is to explore how these heterogeneities in mass transfer couple with heterogeneities in heat transfer within the catalyst pellets and catalyst bed.

Acknowledgements

LFG wishes to take this opportunity to thank David Jackson for the many collaborations and discussions she has had with him over the years. His deep knowledge of applied catalysis has, and will continue to be, of great value to those working in the field.

The authors also wish to thank Shell Global Solutions International B.V. for funding supporting this work. SVE thanks the Sir Winston Churchill Society of Edmonton and the Natural Sciences and Engineering Research Council of Canada for additional financial support. QZ and JWW thank the IChemE Andrew Fellowship for additional financial support.

Author contributions

Conceptualization: SVE, JWW, AJS, CMG, LFG; methodology: SVE, JWW, QZ, AJS; software: SVE; investigation: SVE, JWW, QZ; resources: JWW; writing – original draft: SVE; writing – review & editing: SVE, JWW, CMG, AJS, LFG; supervision: LFG, AJS, MDM, CFG; funding acquisition: LFG, AJS, MDM, CMG.

5 References

[1] E. Stavitski, B.M. Weckhuysen, Infrared and Raman imaging of heterogeneous catalysts, Chem. Soc. Rev. 39 (2010) 4615–4625. https://doi.org/10.1039/C0CS00064G.

[2] M. Gao, H. Li, W. Liu, Z. Xu, S. Peng, M. Yang, M. Ye, Z. Liu, Imaging spatiotemporal evolution of molecules and active sites in zeolite catalyst during methanol-to-olefins reaction, Nat. Commun. 2020 111. 11 (2020) 1–11. https://doi.org/10.1038/s41467-020-17355-6.

[3] L.F. Gladden, Magnetic resonance in reaction engineering: beyond spectroscopy, Curr. Opin. Chem. Eng. 2 (2013) 331–337. https://doi.org/10.1016/j.coche.2013.05.005.

[4] Q. Zheng, J. Williams, L.R. van Thiel, S. V. Elgersma, M.D. Mantle, A.J. Sederman, T.A. Baart, G.L. Bezemer, C.M. Guédon, L.F. Gladden, Operando magnetic resonance imaging of product distributions within the pores of catalyst pellets during Fischer–Tropsch synthesis, Nat. Catal. 2023 62. 6 (2023) 185–195. https://doi.org/10.1038/s41929-023-00913-8.

[5] G.R. Pesch, H. Ridder, C. Sinn, Operando characterization of heterogeneously catalyzed gas- and multi-phase reactions using nuclear magnetic resonance imaging, Chem. Eng. Process. - Process Intensif. 179 (2022) 109086. https://doi.org/10.1016/j.cep.2022.109086.

[6] J. Ulpts, W. Dreher, M. Klink, J. Thöming, NMR imaging of gas phase hydrogenation in a packed bed flow reactor, Appl. Catal. A Gen. 502 (2015) 340–349. https://doi.org/10.1016/j.apcata.2015.06.011.

[7] J. Ulpts, L. Kiewidt, W. Dreher, J. Thöming, 3D characterization of gas phase reactors with regularly and irregularly structured monolithic catalysts by NMR imaging and modeling, Catal. Today. 310 (2018) 176–186. https://doi.org/10.1016/J.CATTOD.2017.05.009.

[8] L.-S. Bouchard, S.R. Burt, M.S. Anwar, K. V. Kovtunov, I. V. Koptyug, A. Pines, NMR imaging of catalytic hydrogenation in microreactors with the use of para-hydrogen, Science. 319 (2008) 442–445. https://doi.org/10.1126/science.1151787.

[9] A.J. Sederman, M.D. Mantle, C.P. Dunckley, Z. Huang, L.F. Gladden, In situ MRI study of 1-octene isomerisation and hydrogenation within a trickle-bed reactor, Catal. Letters. 103 (2005) 1–8. https://doi.org/10.1007/s10562-005-7522-2.

[10] Q. Zheng, F.J. Russo-Abegao, A.J. Sederman, L.F. Gladden, Operando determination of the liquid-solid mass transfer coefficient during 1-octene hydrogenation, Chem. Eng. Sci. 171 (2017) 614–624. https://doi.org/10.1016/j.ces.2017.04.051.

[11] L. Baker, M.P. Renshaw, M.D. Mantle, A.J. Sederman, A.J. Wain, L.F. Gladden, Operando magnetic resonance studies of phase behaviour and oligomer accumulation within catalyst pores during heterogeneous catalytic ethene oligomerization, Appl. Catal. A Gen. 557 (2018) 125–134. https://doi.org/10.1016/j.apcata.2018.03.011.

[12] P.L. Mills, M.P. Dudukovic, A dual-series solution for the effectiveness factor of partially wetted catalysts in trickle-bed reactors, Ind. Eng. Chem. Fundam. 18 (1979) 139–149. https://doi.org/10.1021/I160070A009/ASSET/I160070A009.FP.PNG_V03.

[13] H.S. Fogler, Elements of chemical reaction engineering, 5th ed., Prentice Hall, Hoboken, NJ, USA, 2016.

[14] L. Baussaron, C. Julcour-Lebigue, A.-M. Wilhelm, C. Boyer, H. Delmas, Partial wetting in trickle bed reactors: measurement techniques and global wetting efficiency, Ind. Eng. Chem. Res. 46 (2007) 8397–8405. https://doi.org/10.1021/IE070030B.

[15] L. Baussaron, C. Julcour-Lebigue, A.M. Wilhelm, H. Delmas, C. Boyer, Wetting topology in trickle bed reactors, AIChE J. 53 (2007) 1850–1860. https://doi.org/10.1002/AIC.11189.

[16] Y. Tang, M. Chen, Z. Cheng, T. Yang, B. Chen, H. Ge, X. Fang, Effectiveness factors for a partially wetted catalyst based on the rivulet flow model, Chem. Eng. Sci. 215 (2020) 115515. https://doi.org/10.1016/J.CES.2020.115515.

[17] F. Bazer-Bachi, F. Augier, B. Santos, 1D and 2D simulations of partially wetted catalyst particles: A focus on heat transfer limitations, Chem. Eng. Sci. 66 (2011) 1953–1961. https://doi.org/10.1016/J.CES.2011.01.052.

[18] F. Augier, A. Koudil, A. Royon-Lebeaud, L. Muszynski, Q. Yanouri, Numerical approach to predict wetting and catalyst efficiencies inside trickle bed reactors, Chem. Eng. Sci. 65 (2010) 255–260. https://doi.org/10.1016/J.CES.2009.06.027.

[19] P.A. Ramachandran, J.M. Smith, Effectiveness factors in trickle-bed reactors, AIChE J. 25 (1979) 538–542. https://doi.org/10.1002/AIC.690250321.

[20] J.-D. Grunwaldt, J.B. Wagner, R.E. Dunin-Borkowski, Imaging catalysts at work: a hierarchical approach from the macro- to the meso- and nano-scale, ChemCatChem. 5 (2013) 62–80. https://doi.org/10.1002/cctc.201200356.

[21] C. Chmelik, M. Liebau, M. Al-Naji, J. Möllmer, D. Enke, R. Gläser, J. Kärger, One-shot measurement of effectiveness factors of chemical conversion in porous catalysts, ChemCatChem. 10 (2018) 5602–5609. https://doi.org/10.1002/CCTC.201801530.

[22] B. Sosna, O. Korup, R. Horn, Probing local diffusion and reaction in a porous catalyst pellet, J. Catal. 381 (2020) 285–294. https://doi.org/10.1016/J.JCAT.2019.11.005.

[23] L.F. Gladden, M.D. Mantle, A.J. Sederman, Magnetic resonance imaging of catalysts and catalytic processes, in: Adv. Catal., 2006: pp. 1–75. https://doi.org/10.1016/S0360-0564(06)50001-X.

[24] L.F. Gladden, A.J. Sederman, Magnetic resonance imaging and velocity mapping in chemical engineering applications, Annu. Rev. Chem. Biomol. Eng. 8 (2017) 227–247. https://doi.org/10.1146/annurev-chembioeng-061114-123222.

[25] E.H.L. Yuen, A.J. Sederman, L.F. Gladden, In situ magnetic resonance visualisation of the spatial variation of catalytic conversion within a fixed-bed reactor, Appl. Catal. A Gen. 232 (2002) 29–38. https://doi.org/10.1016/S0926-860X(02)00064-9.

[26] E.H.L. Yuen, A.J. Sederman, F. Sani, P. Alexander, L.F. Gladden, Correlations between local conversion and hydrodynamics in a 3-D fixed-bed esterification process: An MRI and lattice-Boltzmann study, Chem. Eng. Sci. 58 (2003) 613–619. https://doi.org/10.1016/S0009-2509(02)00586-9.

[27] A. Svyatova, E.S. Kononenko, K. V. Kovtunov, D. Lebedev, E.Y. Gerasimov, A. V. Bukhtiyarov, I.P. Prosvirin, V.I. Bukhtiyarov, C.R. Müller, A. Fedorov, I. V. Koptyug, Spatially resolved NMR spectroscopy of heterogeneous gas phase hydrogenation of 1,3-butadiene with para hydrogen, Catal. Sci. Technol. 10 (2020) 99–104. https://doi.org/10.1039/C9CY02100K.

[28] J. Ulpts, W. Dreher, L. Kiewidt, M. Schubert, J. Thöming, In situ analysis of gas phase reaction processes within monolithic catalyst supports by applying NMR imaging

methods, Catal. Today. 273 (2016) 91–98. https://doi.org/10.1016/J.CATTOD.2016.02.062.

[29] I. V. Koptyug, A. V. Kulikov, A.A. Lysova, V.A. Kirillov, V.N. Parmon, R.Z. Sagdeev, NMR imaging of the distribution of the liquid phase in a catalyst pellet during α-methylstyrene evaporation accompanied by its vapor-phase hydrogenation, J. Am. Chem. Soc. 124 (2002) 9684–9685. https://doi.org/10.1021/ja026713u.

[30] K. V. Kovtunov, D. Lebedev, A. Svyatova, E. V. Pokochueva, I.P. Prosvirin, E.Y. Gerasimov, V.I. Bukhtiyarov, C.R. Müller, A. Fedorov, I. V. Koptyug, Robust in situ magnetic resonance imaging of heterogeneous catalytic hydrogenation with and without hyperpolarization, ChemCatChem. 11 (2019) 969–973. https://doi.org/10.1002/CCTC.201801820.

[31] M. Küppers, C. Heine, S. Han, S. Stapf, B. Blümich, In situ observation of diffusion and reaction dynamics in gel microreactors by chemically resolved NMR microscopy, Appl. Magn. Reson. 22 (2002) 235–246. https://doi.org/10.1007/BF03166106/METRICS.

[32] D.B. Burueva, E. V. Pokochueva, X. Wang, M. Filkins, A. Svyatova, S.P. Rigby, C. Wang, G.E. Pavlovskaya, K. V. Kovtunov, T. Meersmann, I. V. Koptyug, In situ monitoring of heterogeneous catalytic hydrogenation via ^{129}Xe NMR spectroscopy and proton MRI, ACS Catal. 10 (2020) 1417–1422. https://doi.org/10.1021/ACSCATAL.9B05000/ASSET/IMAGES/LARGE/CS9B05000_0002.JPEG.

[33] Spectral database for organic compounds SBDS, Natl. Inst. Adv. Ind. Sci. Technol. Japan. (n.d.). https://sdbs.db.aist.go.jp/sdbs/cgi-bin/cre_index.cgi (accessed April 20, 2023).

[34] T.A. Nijhuis, F.M. Dautzenberg, J.A. Moulijn, Modeling of monolithic and trickle-bed reactors for the hydrogenation of styrene, Chem. Eng. Sci. 58 (2003) 1113–1124. https://doi.org/10.1016/S0009-2509(02)00547-X.

[35] J.P. White, T.W. Chamberlain, R.A. Bourne, D. Taylor, C. Brennan, F.L. Muller, Decoupling the relative rate of hydrogen uptake via convection and mass transfer by a single catalytic pellet in a scaled down trickle bed reactor, Chem. Eng. J. 394 (2020) 124290. https://doi.org/10.1016/J.CEJ.2020.124290.

[36] I. Stamatiou, F.L. Muller, Determination of mass transfer resistances in trickle bed reactors, Chem. Eng. J. 377 (2019) 119808.

[37] A. Gianetto, V. Specchia, Trickle-bed reactors: state of art and perspectives, Chem. Eng. Sci. 47 (1992) 3197–3213. https://doi.org/10.1016/0009-2509(92)85029-B.

[38] J. Fernengel, L. Bolton, O. Hinrichsen, Characterisation and design of single pellet string reactors using numerical simulation, Chem. Eng. J. 373 (2019) 1397–1408. https://doi.org/10.1016/J.CEJ.2019.03.114.

[39] T.R. Brown, B.M. Kincaid, K. Ugurbil, NMR chemical shift imaging in three dimensions., Proc. Natl. Acad. Sci. 79 (1982) 3523–3526. https://doi.org/10.1073/PNAS.79.11.3523.

[40] J. Hennig, A. Nauerth, H. Friedburg, RARE imaging: A fast imaging method for clinical MR, Magn. Reson. Med. 3 (1986) 823–833. https://doi.org/10.1002/mrm.1910030602.

[41] S. Meiboom, D. Gill, Modified spin-echo method for measuring nuclear relaxation times, Rev. Sci. Instrum. 29 (1958) 688–691. https://doi.org/10.1063/1.1716296.

[42] H.Y. Carr, E.M. Purcell, Effects of diffusion on free precession in nuclear magnetic resonance experiments, Phys. Rev. 94 (1954) 630–638. https://doi.org/10.1103/PhysRev.94.630.

[43] R. Cotts, M. Hoch, T. Sun, J. Markert, Pulsed field gradient stimulated echo methods for improved NMR diffusion measurements in heterogeneous systems, J. Magn. Reson. 83 (1989) 252–266. https://doi.org/10.1016/0022-2364(89)90189-3.

[44] K. Karlsons, D.W. De Kort, A.J. Sederman, M.D. Mantle, H. De Jong, M. Appel, L.F. Gladden, Identification of sampling patterns for high-resolution compressed sensing MRI of porous materials: 'learning' from X-ray microcomputed tomography data, J. Microsc. 276 (2019) 63–81. https://doi.org/10.1111/jmi.12837.

[45] M. Lustig, D. Donoho, J.M. Pauly, Sparse MRI: The application of compressed sensing for rapid MR imaging, Magn. Reson. Med. 58 (2007) 1182–1195. https://doi.org/10.1002/mrm.21391.

[46] M. Benning, L. Gladden, D. Holland, C.B. Schönlieb, T. Valkonen, Phase reconstruction from velocity-encoded MRI measurements - A survey of sparsity-

promoting variational approaches, J. Magn. Reson. 238 (2014) 26–43. https://doi.org/10.1016/j.jmr.2013.10.003.

[47] D.W. de Kort, A. Reci, N.P. Ramskill, M. Appel, H. de Jong, M.D. Mantle, A.J. Sederman, L.F. Gladden, Acquisition of spatially-resolved displacement propagators using compressed sensing APGSTE-RARE MRI, J. Magn. Reson. 295 (2018) 45–56. https://doi.org/10.1016/j.jmr.2018.07.012.

[48] N. Otsu, A threshold selection method from gray-level histograms, IEEE Trans. Syst. Man. Cybern. 9 (1979) 62–66. https://doi.org/10.1109/TSMC.1979.4310076.

[49] J. Rgzieka, J. Hanikab, caysls today Partial wetting and forced reaction mixture transition in a model trickle-bed reactor, Catal. Today. 20 (1994) 467484.